CrossMark

Optimizing the thermal annealing temperature: technological route for tuning the photo-detecting property of p-CuO thin films grown by chemical bath deposition method

Jenifar Sultana[1] · Somdatta Paul[1] · Anupam Karmakar[2] · Goutam K. Dalapati[3] · Sanatan Chattopadhyay[2]

Abstract

In the current work, CuO thin films (~ 110 nm) are grown by employing chemical bath deposition (CBD) method on Si substrate for fabricating the p-CuO/n-Si heterojunction photodetectors. The as-grown films are annealed at 250, 550 and 850 °C for 10 min in Ar ambient for tuning optoelectronic properties of the as-grown CuO thin films. Comparative study on systematic annealing of the film within 250–550 °C indicates a morphological change of the as-grown CuO film to nano-fiber type with its chemical composition remaining unchanged. A variation of refractive index and dielectric constant in the range of 2.65–2.93 and 7.2–9.7, and a change of absorption coefficient and bandgap from 1.33×10^5 to 6.06×10^5 cm^{-1} and 1.5 to 2.16 eV have been observed. The current–voltage characteristics both in dark and illuminated conditions suggest that the annealing of CuO film at 550 °C provides the best performance in terms of photo-to-dark current ratio and photoresponsivity. A respective enhancement of 5.07 and 10% for the photo-to-dark ratio and photoresponsivity has been observed for the 550 °C annealed sample.

1 Introduction

Metal-oxide thin films have drawn noteworthy research interests in recent years due to their multifaceted applications in the areas of electronics, optoelectronics, energy scavenging and catalysis [1–3, 16]. In this context, copper

✉ Sanatan Chattopadhyay
  scelc@caluniv.ac.in

  Jenifar Sultana
  sultanajenifar@gmail.com

  Somdatta Paul
  paul.somdatta@gmail.com

  Anupam Karmakar
  akelc@caluniv.ac.i

  Goutam K. Dalapati
  dalapatig@imre.a-star.edu.sg

1 Centre for Research in Nanoscience and Nanotechnology (CRNN), Kolkata 700098, India

2 Department of Electronic Science, University of Calcutta, 92, A.P.C. Road, Kolkata 700009, India

3 Institute of Materials Research and Engineering, A*STAR (Agency for Science, Technology and Research), 2 Fusionopolis Way; Innovis, #08-03, Singapore 138634, Singapore

oxide is gaining more and more attention due to its unique physical and chemical properties and cost-effective growth/deposition technology [3, 4]. It finds wide range of applications in the domain of energy harvesting and storage [5], photo-electro-chemical cells [6], photo-catalysts [1, 2, 7], batteries [8], field-emission devices [9], gas sensors [2], photovoltaic devices [10], and superconductors [11]. It has also huge potential for bio-medical/biological applications due to its non-toxic nature [1, 10].

Copper oxides can be of two types: the tenorite (CuO) and cuprite (Cu$_2$O) [3], and both have semiconducting nature with promising electrical and optical properties [10]. Both the cupric- oxide (CuO) and cuprous-oxide (Cu$_2$O) are II–VI p-type semiconductors in general and hence potentially useful for developing different electronic devices. Cuprous oxide is reported to be a direct bandgap semiconductor with a bandgap of 2 eV while cupric oxide is of monoclinic structure with a direct bandgap of 1.21–1.51 eV [10, 12]. The relatively smaller band gap of CuO makes it a potentially superior material for photo-detection and optical switching applications in the visible or near-infrared region [12]. Moreover, since solar spectrum comprises of both UV and visible wavelengths, significant research efforts are being made to design photodetectors to absorb the entire solar spectrum [5]. In this context, the responsivity of CuO based

photodetectors can be further increased by incorporating a wide band-gap semiconductor, such as, n-ZnO due to its direct band gap of 3.37 eV. Recently, a photovoltaic device with the combination of p-type copper oxide (CuO) and n-type Zinc oxide (ZnO) has been reported with superior performance [12].

The chemical and physical properties of such thin films depend on their thickness and morphology which change significantly with thermal treatment due to subsequent processing [12]. Reports are also available to indicate that the electrical and optical properties of the devices based on these films depend significantly on their thicknesses, and therefore, the thickness has been optimized for superior optoelectronic performance [3]. Thus, investigation of the morphological changes during subsequent thermal treatment at different temperatures on such optimized CuO films is immensely crucial for their appropriate use in the areas of nano-electronics, optoelectronics and bio-sensing. Also, there are few reports available in literature, based on the effect of annealing temperature of CuO. However, most of them reported the impact of annealing up to 500 °C and shown that the photovoltaic performance and the film crystallinity improves upon annealing [12, 30]. Thus, investigating the optimized annealing temperature at which the CuO film has the best optimized photovoltaic performance is immensely vital for the optoelectronic applications.

The thin films of copper oxide can be grown by adopting different techniques including the reactive sputtering [13], chemical vapor deposition (CVD) [14], chemical conversion [15], vapor liquid solid [16], thermal oxidization [17], rapid precipitation, spin coating [18], solid state reaction [19], sono-chemical reaction, sol–gel techniques [20], solvo-thermal route [21], electrochemical route [22], spray pyrolysis, thermal oxidation and hydrothermal method [23]. Also, the performance of such films developed by each of these individual techniques has been reported [13, 24]. In this context, the chemical bath deposition (CBD) is a growth process that has drawn significant attention due to its simplicity, cost-effectiveness, reproducibility and capability of large area scaling for commercial production [3, 25, 26]. The deposition rate and hence thickness of the deposited film can be precisely controlled by varying pH, temperature and concentration of the solution.

In the current work, thin films of CuO are grown by employing chemical bath deposition process on n-Si <100> substrates. The grown CuO films are furnace annealed at 250, 550 and 850 °C for 10 min in Argon environment. Morphological changes of the heat-treated films are investigated from SEM micrograph analysis and their crystallite quality is studied from X-ray diffraction pattern. The refractive index (n), static and high-frequency dielectric constants (ε_o and ε_{hf}), absorption coefficient (α) and bandgap energy (E_g) of the as-grown and annealed films are investigated by using spectroscopic ellipsometer. The electronic and optoelectronic performance of the p-CuO/n-Si hetero-junction diodes are performed by measuring its rectification properties, barrier height, ideality factor and photo-detection properties.

2 Experimental

Chemical bath deposition technique has been employed for growing thin film of CuO on n-Silicon (Si) <100> substrate. The Si wafers are initially cleaned by following the RCA-I and RCA-II steps and then immersed into 20% HF solution for native oxide removal. The 0.1 M $CuCl_2 \cdot 2H_2O$ is used as the source of Cu^{2+} in the CBD solution and ammonium hydroxide (NH_4OH) solution is used as a precursor which is added drop-wise. The volume of the CBD growth solution is ~100 mL and the cleaned Si substrates are placed in a Teflon holder to immerse into the solution. The beaker containing the solution is then placed on the hot plate under constant stirring and heated from room temperature to ~60 °C at a rate of 5°C/min. When the temperature of the bath is reached to ~60 °C, then 5 ml of ammonia solution is added drop-by-drop to the reaction mixture. After the addition of ammonia solution, the bath is again heated until its temperature rises to ~85 °C. At that instant, the temperature settings of the hot plate are adjusted to maintain a steady heating condition for up to ~15 min until the solution colour changes to black which also indicates the formation of CuO phase. After the formation of CuO phase, the as-deposited sample has been grown for 10 min. The as-deposited CuO films on Si substrates are then taken out from the beaker, and thoroughly rinsed in DI water to remove the residual solutes and impurities from the surface [1]. The samples are then further sonicated in DI water for 10 min to remove the non-adherent particulates and finally dried up by blowing nitrogen gas.

The as-deposited sample is then broken into four pieces for investigating the impact of annealing temperature on such CBD grown samples. One of the as-deposited samples is kept unprocessed and the rests are annealed in argon (Ar) environment in a furnace for 10 min at 250, 550 and 850 °C, respectively. The as-deposited and post-annealed samples are characterized by employing structural, optical and electrical techniques. An ITO layer of thickness 100 nm is evaporated on the CuO film followed by the formation of Al dots on it to take electrical contact having an effective device area of 2.06×10^{-3} cm^2 of the p-CuO/n-Si diodes. The chemical nature and oxidation states of copper on the surface of as-deposited and annealed samples are examined by XPS analysis. The XPS data are deconvoluted using Peak Fit software (Version-4.12). Spectroscopic ellipsometry (SE) is used to analyze different optical parameters such as refractive index (n), absorption coefficient (α), static and high frequency dielectric constant (ε_0 and ε_∞) and optical band gap

(E_g) of both the as-deposited and annealed CuO thin films on Si substrate. The current–voltage (I–V), photo-switching and spectral response (responsivity) measurements of the p-CuO/n-Si heterojunctions are performed by using Keithley 4200-SCS Parameter Analyzer. The photo-detecting (responsivity) measurements are done under the illumination of 100 mW/cm^2 incident light power (Model No. LCS-100 Series Small Area Solar Simulator, Oriel Instruments) coupled with the source meter and a monochromator.

3 Results and discussion

3.1 Structural and material characterization of p-CuO thin film grown on n-Si

Figure 1a–d shows the SEM micrographs of the as-deposited, 250, 550 and 850 °C annealed samples, respectively. SEM image of the as-deposited sample indicates the formation of a non-uniform film with no well defined grain boundaries however, after annealing at 250 °C, the morphology is changed to nano-fibre type. This is a thermodynamically driven process and can be explained as follows: the atoms at the surface of the as-deposited film are energetically less stable. Upon annealing, as the system tries to lower its overall energy, molecules on the surface of the film will tend to detach from the surface. When all small particles do this, it increases the concentration of free molecules. When the free molecules are supersaturated, they have a tendency

to condense on the surface forming larger particles. Thus, all smaller particles shrink, while larger particles grow, and overall the average size will increase. With the increase of annealing temperature to 550 °C, the nano-fibre shaped structures coalesce to form relatively larger nano-structures, as depicted in Fig. 1(c).

However, the micrograph of Fig. 1d obtained for 850 °C annealed sample indicates the formation of a uniform film where the nanostructures are agglomerated to form larger structures which may be attributed to larger surface tension working over the films [27]. Such formation of film at relatively higher annealing temperature is due to the thermodynamic preference of energy lowering by minimizing total surface area of the structures. Consequently, all the nanostructures coalesce to form a film-like morphology at higher annealing temperature.

The EDAX spectra of as-deposited CuO thin film and those for the samples annealed at different temperatures are measured by employing JEOL-JSM 7600F FESEM system and are shown in Fig. 2a. It is apparent from elemental plots that the ratio of Copper and Oxygen is ~ 1:1, and hence, confirms the formation of appropriate stoichiometric CuO film. Further, it would be relevant to mention that the intensity of Si peak in EDAX spectra of both the as-deposited and 850 °C annealed samples is much higher in comparison to Copper and Oxygen. This may be attributed to the porous CuO film through which more electrons reach up to the Si substrate. In comparison, the 250 and 550 °C annealed samples exhibit high intensity peaks for Cu and O than Si

Fig. 1 FESEM images of the CBD grown CuO thin films for the: **a** as-deposited; **b** 250 °C annealed; **c** 550 °C annealed and; **d** 850 °C annealed samples
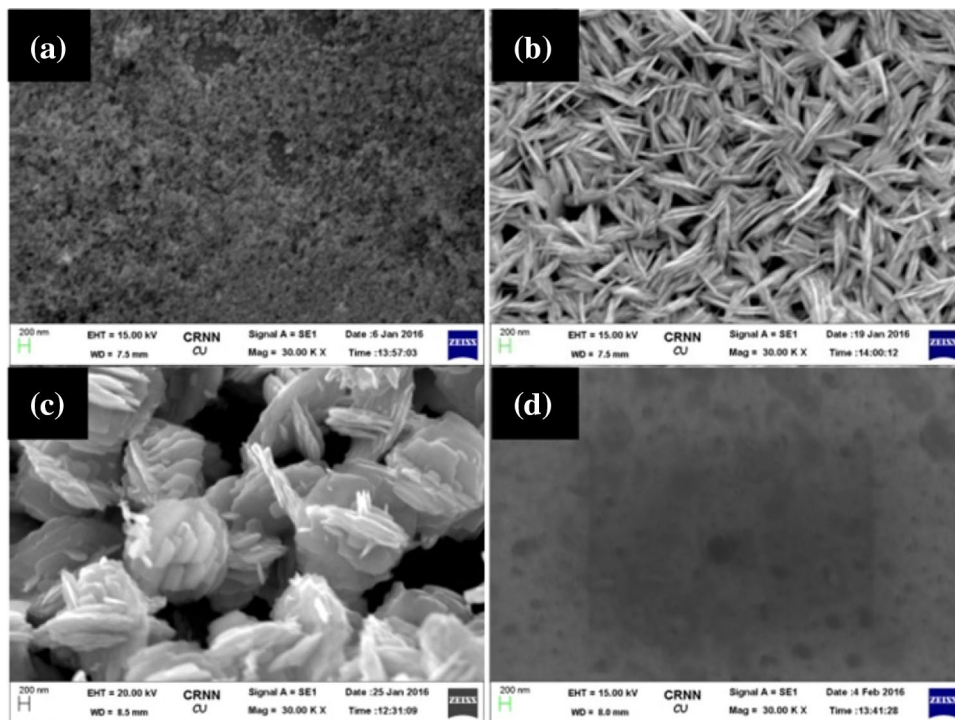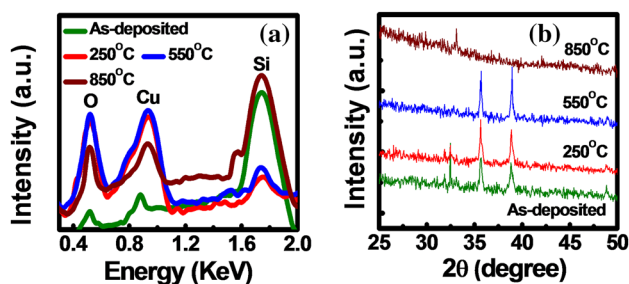
Fig. 2 **a** Comparative plots of EDAX spectra for the as-deposited and 250, 550 and 850 °C annealed samples; **b** comparative plots of XRD patterns for the as-deposited, 250, 550 and 850 °C annealed samples

which corroborate the higher surface area covered by the nano-structures formed during annealing. Therefore, the composition of CuO phase remains unchanged even after annealing at 850 °C [28].

To investigate the crystallographic as well as structural orientation of the grown samples, X-ray diffraction measurements are performed and the relevant spectra are plotted in Fig. 2b for the as-deposited and annealed samples. The samples exhibit diffraction peaks that confirm the formation of monoclinic CuO, verified by JCPDS card no. 80-1917. Figure 2b suggests an increase in intensities and decrease of widths (FWHM) of the X-ray peaks for the annealed samples up to 550 °C, thereby, confirms the improvement of crystalline quality of the CBD grown samples due to annealing. However, the decrease in peak intensity and increase in FWHM for 850 °C annealed sample suggest a degradation of crystalline quality which may be attributed to the conversion of its main [002] plane to [110] plane [28].

The average crystallite size and micro-strain has been calculated and are summarized in Table 1. As expected, the lattice strain has decreased with the increase of crystallite size which suggests the improved orientation of CuO crystallites upon annealing at 550 °C [29].

The elemental composition and chemical states of the as-deposited and annealed samples are analyzed by X-ray

photoelectron spectroscopy and the results are shown in Figs. 3a, b, 4a–d, 5 and 6a–d. Figure 3a shows the high resolution Cu 2p doublet X-ray photoelectron spectra for the as-deposited and annealed films. Also in order to get more information about the oxidation states of Cu, the main Cu $2p_{3/2}$ photoelectron peak along with its satellite are deconvoluted and are shown in Fig. 4a–d, respectively. The XPS spectra of all the samples show the main Cu $2p_{3/2}$ photoelectron peak and its satellite, where the latter being indicative of Cu^{+2} state [3, 30].

Also it is worthy to note that except the film annealed at 550 °C, the as-deposited and all other annealed films comprise of two kinds of phases: a $2p_{3/2}$ peak of Cu^0/Cu^+ located at ∼ 932 eV and the Cu^{2+} $2p_{3/2}$ peak located at ∼ 933.4 eV .

However, comparison between the spectra of as-deposited and annealed samples exhibit significant changes in relative intensity of satellite to the main peak. Also, there is an obvious shift in the $Cu2p_{3/2}$ main peak binding energy which may be attributed to the change in Cu^{2+} and/or Cu^0/Cu^+ composition at the film surface with annealing temperature.

The ratio of integrated areas under the main and satellite peaks are used to demonstrate the impact of Cu^{2+} and/ or Cu^0/Cu^+ at the surface of the as-deposited and annealed films. Therefore, for developing an inclusive idea about the
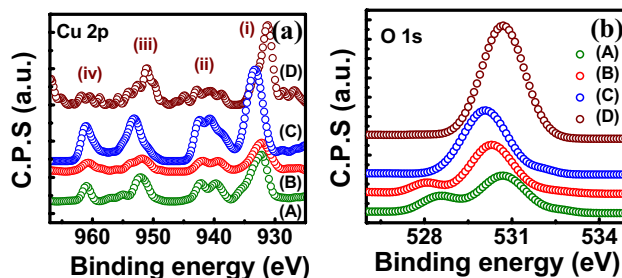

Fig. 3 **a** Cu 2p X-ray photoelectron spectra of the as-deposited and annealed CuO films showing: (i) Cu $2p_{3/2}$ main peak; (ii) satellite line of Cu $2p_{3/2}$; (iii) Cu $2p_{1/2}$ main peak and (iv) satellite line of Cu $2p_{1/2}$; **b** O 1s XPS spectra for the: (*A*) as-deposited; (*B*) 250 °C annealed; (*C*) 550 °C annealed; and (*D*) 850 °C annealed samples

Table 1 Summary of the parameters extracted from X-ray diffraction analysis

| Sample (ID)	Peak position (deg.)	FWHM (deg.)	d-spacing (Å)	Crystallite size (nm)	Micro-strain
As-deposited	35.689 [002]	0.1948	2.517	29.00	0.0026
	38.861 [111]	0.1258	2.316	21.33	0.0032
	32.574 [110]	0.1299	2.308	43.75	0.0020
250 °C annealed	35.672 [002]	0.1598	2.517	35.42	0.0022
	38.882 [111]	0.1948	2.316	29.33	0.0024
	32.574 [110]	0.1342	2.931	41.75	0.0021
550 °C annealed	35.687 [002]	0.1548	2.516	36.57	0.0021
	38.913 [111]	0.1598	2.314	35.76	0.0020
850 °C annealed	32.564 [110]	0.1548	2.514	36.56	0.0021
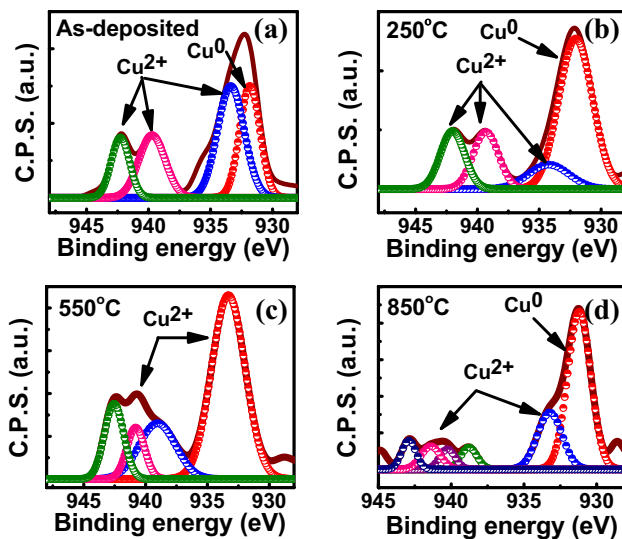
Fig. 4 Deconvoluted X-ray photoelectron spectra for the Cu $2p_{3/2}$ main line and its corresponding satellite line of **a** as-deposited; **b** 250 °C annealed; **c** 550 °C annealed and **d** 850 °C annealed samples
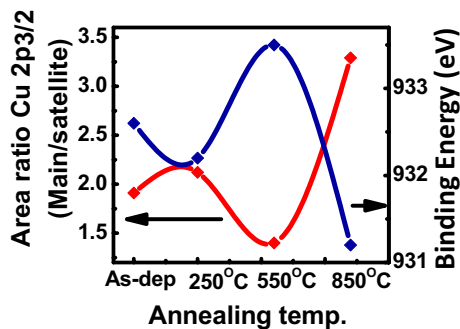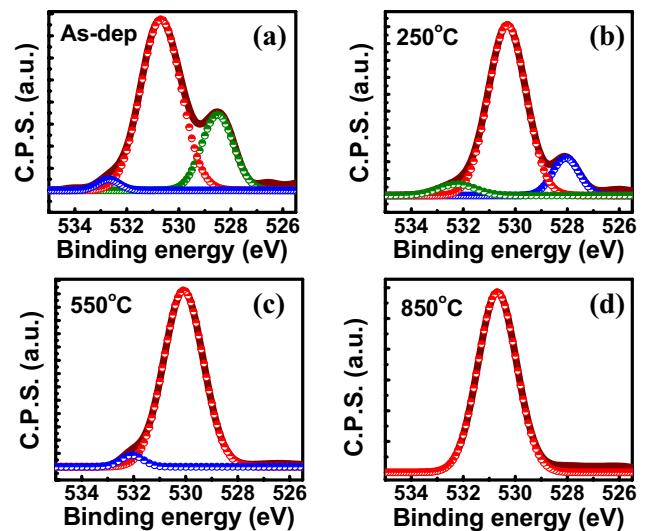

Fig. 6 Deconvoluted O 1s X-ray photoelectron spectra of: **a** as-deposited; **b** 250 °C annealed; **c** 550 °C annealed and **d** 850 °C annealed samples

Fig. 5 Effect of annealing in Cu^{2+} surface concentration as represented by Cu $2p_{3/2}$ main to satellite peak area ratio and Cu $2p_{3/2}$ main peak binding energy

amount of Cu^{2+} and/or Cu^0/Cu^+ phase at the film surface, the area-ratio of Cu 2p peak (main/satellite) and Cu 2p main peak binding energy is plotted for different samples in Fig. 5. The value of area-ratio of the main and satellite peaks of Cu $2p_{3/2}$ is observed to increase first for the 250 °C annealed sample, then becomes a minimum for 550 °C annealed sample and finally, attains a maximum value upon subsequent annealing at 850 °C. It is reported that the Cu^{2+} represents both the satellite and main peak whereas Cu^0 and/or Cu^+ contribute to the main peak only [31]. The trend of area-ratio, as revealed from Fig. 5, is attributed to the decreasing importance of Cu^{2+} and/or an increasing importance of Cu^0/Cu^+ in the surface region of the 250 and 850 °C annealed samples. The decrease in the area-ratio of 550 °C annealed sample can be attributed to the formation of maximum amount of Cu^{2+} phase. The
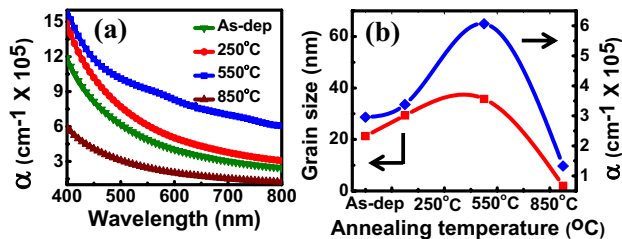
similar trend about the oxidation state of Cu in the surface layer is also observed from the plot of Cu 2p main peak binding energy with annealing temperature. Thus, it is clear from the Cu 2p XPS study that on annealing the as-deposited sample at 550 °C, only Cu^{2+} exists and hence gives superior photovoltaic performance as compared to all other samples.

Typical O 1s spectra and the corresponding deconvoluted spectra of as-deposited and annealed samples are shown in Figs. 3b and 6a–d, respectively. It is evident from Fig. 6a–d that the main peak at ~ 530.3 eV for all the samples is originated from the lattice oxygen O^{2-}. For the as-deposited and 250 °C annealed samples the peak at 528.1 eV is also attributed to the O^{2-} phase. Further, the broad peak at 532.3 eV for all the samples except the one annealed at 850 °C is attributed to the adsorbed oxygen in the surface of the film [32, 33]. Since the contribution of lattice oxygen O^{2-} is more than 90% of the total O 1s intensity in all the cases, the entire area of O 1s peak is taken as the denominator to express "copper-to-oxygen" ratios for the film surfaces.

It will also be more informative if the numerators in such ratios are the integrated areas of Cu^{2+} and Cu^0/Cu^+ peaks other than the integrated area of Cu $2p_{3/2}$ main peak, since the latter does not discriminate between Cu^{2+} and/or Cu^0/Cu^+ phases. Values of all such relevant ratios are computed for all the samples and have been summarized in Table 2. It is apparent from Table 2 that a proper stoichiometric CuO film surface is formed on annealing the as-deposited film at 550 °C and such results corroborate with those of XRD analysis.

Table 2 Comparison of relative surface concentration of oxygen, Cu^{2+}, Cu^0/Cu^+ and total Cu and their corresponding normalized ratios of the as-deposited and annealed samples

Sample	Normalized peak areas and their ratios							
	O1s	Cu^{+2}	Cu^0 or Cu^+	Cu_{Total}	$\frac{Cu^0 \text{ or } Cu^+}{O1s}$	$\frac{Cu^{2+}}{O1s}$	$\frac{Cu_{Total}}{O1s}$	$\frac{Cu^0 \text{ or } Cu^+}{Cu^{2+}}$
As-dep	0.069	0.39	0.268	0.658	03.88	5.65	09.53	0.690
250 °C	0.070	0.44	1.000	1.440	14.30	6.28	20.57	2.270
550 °C	1.000	1.00	0	1.000	0	1.00	1.00	0
850 °C	0.710	0.16	0.340	0.500	0.48	0.22	0.70	2.125

Fig. 7 a Plots of the extracted absorption coefficient with wavelength for the as-deposited and annealed samples and; **b** variation of grain size and absorption coefficient with annealing temperature

3.2 Optical characterization of p-CuO thin film grown on n-Si

Spectroscopic Ellipsometric (SENTECH SE850) measurement is performed in the spectral range of 400 nm to 800 nm for obtaining Ψ [the amplitude ratio between reflected and polarized component (p)] and Δ (phase difference between the reflected and polarized component) for the 60° angle of incidence. The measured ellipsometric parameters Ψ and Δ are utilized to determine the values of extinction coefficient (k) for both the as-deposited and annealed CuO films. The absorption coefficients of the as-deposited and annealed films are extracted from the measured extinction coefficient, by using the formula:

$$\alpha = \frac{4\pi k}{\lambda},\tag{1}$$

where k is the extinction coefficient and λ is the wavelength of the incident photon. The variation of absorption coefficients of the as-deposited and annealed films with wavelength are shown in Fig. 7a. The 550 °C annealed sample is observed to exhibit the highest absorption coefficient within the wavelength range considered which may be attributed to the highest amount of CuO phase formed and highest grain size of the dominating [002] plane as observed from SEM, XRD and XPS analyses.

The bandgap of such grown films is also extracted by using Tauc's relation [34]:

$$\alpha h v = A \left(h v - E_g \right)^n \tag{2}$$

where α is the absorption coefficient in cm^{-1}, hv is the photon energy, E_g is the energy gap, A is the energy dependent constant and the value of n depends on the nature of electronic transition (½ for direct allowed transition).

The energy bandgap of the as-deposited and 250, 550 and 850 °C annealed CuO thin films is estimated to be 1.75, 1.66, 1.5 and 2.16 eV, respectively. The bandgap energy of bulk CuO is reported to be in the range of 1.2–1.5 eV [28] and relatively higher bandgap for the current structure is attributed to the effect of quantum confinement, which is usually observed in 1-D nanostructure [35]. The bandgap energy values are observed to decrease with increasing annealing temperature and attain a minimum of 1.5 eV for 550 °C annealed sample, however, for the 850 °C annealed sample the bandgap is obtained to be 2.16 eV. This can be attributed to the enhancement of CuO phase due to annealing at 550 °C, however, it is minimum for 850 °C annealed sample which has also been observed from XPS analysis. This band gap shift can also be explained from the crystallite size of the dominating CuO phase in the sample which has been extracted from XRD results.

The obtained result complies with the effective mass theory (EMA), which predicts r^{-2} dependence of the bandgap, with r^{-1} correction term in the strong confinement regime, where r is the crystallite size. As mentioned earlier, the crystallite size increases with the increase of annealing temperature up to 550 °C which results to decrease the bandgap energy according to the effective mass theory (EMA) [36]. The variation of grain size of the dominant phase and the absorption coefficient corresponding to the bandgap energy value with annealing temperature are plotted in Fig. 7b. The minimum and maximum absorption coefficients are obtained for the 850 and 550 °C annealed samples, respectively. The results are analogous with the grain size of the dominant [002] plane as obtained from XRD results.

The plot of refractive index as a function of photon energy is shown in Fig. 8a which indicates the refractive index depends on the annealing temperature as well as film morphology. The refractive indices are determined by using Moss relation and Herve-Vandamme relation [37]:
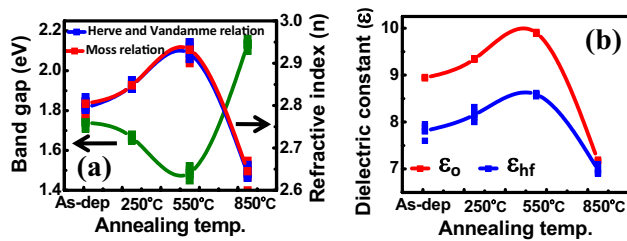
$$n^2 = \sqrt{\frac{k}{E_g}} \tag{3}$$

Fig. 8 **a** Variation of refractive index and energy bandgap of the CuO films and; **b** the variation of ε_o (static) as well as ε_{hf} (high frequency) dielectric constants of the as-deposited and annealed CuO films

where k is a constant with a value of 108 eV and

$$n = \sqrt{1 + \left(\frac{A}{E_g + B}\right)^2} \qquad (4)$$

where A and B are numerical constants with values 13.6 and 3.4 eV, respectively.

The values of refractive index are extracted to be 2.81, 2.85, 2.93 and 2.65 for the as-deposited and 250, 550 and 850 °C annealed samples, respectively. Since refractive index indicates quality of the grown films, the higher refractive index confirms the formation of highly dense films with excellent crystalline structure upon annealing at 550 °C [27]. This is in collaboration with the XRD analysis which also reveals the improvement of crystallite size upon annealing at 550 °C. Also, the refractive index values of the as-deposited and annealed CuO films corroborate well with the literature values [27, 38]. The CuO thin film annealed at 550 °C exhibits the highest refractive index compared to other annealed samples and thereby indicates its suitability to use as the anti-reflection coating material [38].

The dielectric constant is one of the fundamental intrinsic material properties [27] and it is also associated with the property of altering (slowing down) the speed of light in the material. The static dielectric constant (ε_o) and high-frequency dielectric constant (ε_{hf}) are extracted by using the relation between the film permittivity, refractive index and its energy bandgap [37]. Figure 8b shows the plot of static and high frequency dielectric constant for the as-deposited and annealed films. The dielectric constant increases upon annealing as compared to the as-deposited sample and the maximum value of dielectric constant is observed to be 9.7 for 550 °C annealed film. It is worthy to mention that the band gap, refractive indices and dielectric constant values have been measured for 5 different samples corresponding to each annealing temperature to verify the repeatability and reliability of the results and a maximum spread of ±3.4% in the results has been observed which suggests a good reproducibility of the results.
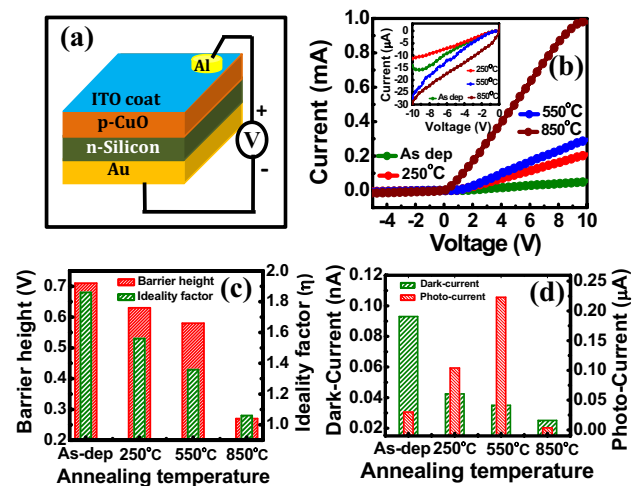

Fig. 9 **a** Schematic of the fabricated device, **b** plots of I–V characteristics under dark condition (linear scale); inset shows the magnified values of reverse biased current; **c** variation of ideality factor and barrier height with annealing temperature and; **d** variation of dark-current and photo-current at 0 V bias of the devices for as-grown, 250, 550 and 850 °C annealed samples

3.3 Electrical characterization of the fabricated heterojunctions

Schematic diagram of the fabricated p-CuO/n-Si heterojunction diode is shown in Fig. 9a. The electrical characterization of such devices is performed by measuring the relevant current–voltage (I–V) characteristics, shown in Fig. 9b, and the magnified version of its reverse biased currents are shown in the inset. The I–V plots indicate an increase of current with annealing temperature under forward bias. The barrier height and ideality factor of all the diodes are extracted from such I–V characteristics and are plotted in Fig. 9c. Both the barrier height and ideality factor are observed to decrease with increasing annealing temperature and hence confirms the formation of superior heterojunction on 850 °C annealed film. This may be attributed to the reduction of series resistance with increasing annealing temperature. Figure 9d shows the comparative plots of dark- and photo- current at 0 V bias for the as-grown, 250, 550 and 850 °C annealed samples. The maximum photo-current of 2.23×10^{-7} A with a photo-to-dark current ratio of 6371 has been obtained for the 550 °C annealed sample.

The presence of series resistance (R_s) is very important since the net applied voltage across a diode is divided between its depletion layer and series bulk resistance. The values of such shared voltage drop depend on the depletion layer thickness and R_s, thereby, control the performance and reliability of these devices.

Series resistance values are determined from the inverse slope of I–V characteristics ($R_i = dV_i/dI_i$), under dark
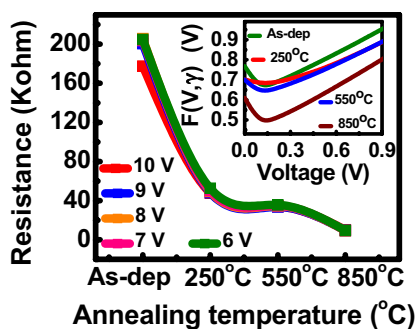
Fig. 10 Variation of resistance with annealing temperature at different voltage (inset shows the corresponding Norde's plot)
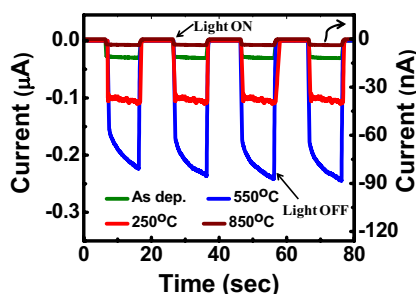

Fig. 11 Plot of light 'ON'/'OFF' switching characteristics of the heterojunction photodiode at 0 V bias

condition as shown in Fig. 10, and is found to have a minimum value of 9.2 K for 850 °C annealed sample. The relevant modified Norde's plots are also shown at the inset of Fig. 10. By using Norde's plot the value of series resistance is calculated to be ~9.48 K for the 850 °C annealed sample.

To investigate the photo-detection characteristics of the grown heterojunctions, time-dependent photocurrent is measured by switching the white light source (in-built with the probe station), 'ON' and 'OFF' periodically for cycles of 20 s each and are shown in Fig. 11. The relevant rise-time and fall-time are calculated from such data and are found to be minimum for 550 °C annealed sample. The light 'ON'/'OFF' characteristics indicate that such heterojunctions can also be used for photo-detection.

Table 3 compares the band gap (E_g), barrier height (ϕ_B), ideality factor (n), rise-time, fall-time, dark-current at 0 V, photocurrent generated at 0 V bias and photo-to-dark current ratio with annealing temperature of the p-CuO/n-Si heterojunction diode.

Rise-time and fall-time are observed to decrease with annealing temperature up to 550 °C, however, it has been observed to be maximum for 850 °C annealed sample. Also, the photocurrent generated at 0 V bias is the maximum for 550 °C annealed samples. The comparatively faster response of 550 °C annealed samples is attributed to the fact that the photo-response vary with the amount of input light absorption by CuO films which depends on its morphology. Significant morphological changes have been observed from SEM images (Fig. 1) for the as-deposited and 250, 550 and 850 °C annealed samples. Upon annealing at 250 °C, a crystalline nano-fibre type structures are formed which agglomerate to form nano-crystals after annealing at 550 °C. Such nanostructures increase the effective area for light absorption and lead to enhance the photo-response in comparison to the as-deposited sample [39]. Due to further high temperature annealing at 850 °C, the individual nano-crystals conglomerate to reconstruct the film with superior surface morphology compared to the as-deposited sample. This enhances reflection of the incident light from the surface and thereby reduces its effective absorption. Also, the SEM image of Fig. 1d and relevant EDAX data for 850 °C annealed sample indicated the exposure of more Si area which have also reduced the amount of effective light absorption in CuO layer, and thus, degrades the photo-responsivity [24].

To demonstrate the effectiveness of the fabricated p-CuO/n-Si heterojunction photodetectors, the spectral response has been measured at 0 V bias under illumination of different wavelength light (300–1000 nm) and is shown in Fig. 12a.

It is observed from the plot that the annealing temperature has significant impact on the responsivity of the p-CuO/n-Si system. The CuO film annealed at 550 °C shows relatively higher photo-response as compared to other samples considered in the current work. This is attributed to the enhanced absorption by the nanostructures formed upon annealing at 550 °C as confirmed from SEM (Fig. 1) and SE (Fig. 7)

Table 3 The comparison of band gap (E_g), barrier height (ϕ_B), ideality factor (n), rise-time, fall-time, dark current at 0 V, photocurrent (at 0 V bias) and photo-to-dark current ratio with annealing temperature

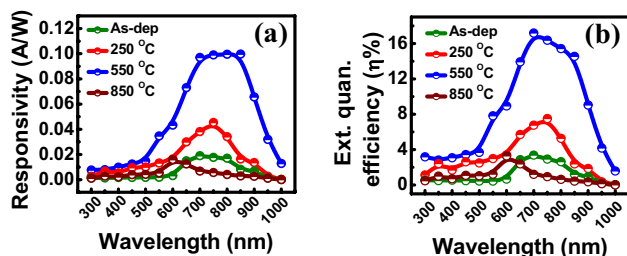| Sample (ID)	E_g (eV)	ϕ_B (eV)	Ideality factor (n)	Rise-time (sec)	Fall-time (sec)	Dark-current at 0 V (A)	Photo-current at 0 V (A)	Photo-to-dark current ratio
As-dep	1.75	0.71	1.56	1.34	1.35	9.30E−11	3.00E−8	323
250 °C	1.66	0.63	1.36	1.2	1.21	4.24E−11	1.04E−7	2453
550 °C	1.50	0.60	1.32	0.85	0.83	3.50E−11	2.23E−7	6371
850 °C	2.16	0.58	1.06	1.70	1.79	2.51E−11	3.50E−9	139

Fig. 12 a Variation of responsivity and; **b** external quantum efficiency with wavelength (300–1000 nm) at 0 V for the as-deposited, 250 °C annealed, 550 °C annealed and 850 °C annealed samples

analysis. Also, it is observed from the responsivity plot that photocurrent initially increases upto a certain wavelength and then decreases sharply. This cut-off wavelength is measured to be 700 nm (1.77 eV), 750 nm (1.65 eV), 850 nm (1.45 eV) and 600 nm (2.06 eV), for the as-deposited, 250, 550 and 850 °C annealed samples, respectively. It is worthy to note that this cut-off wavelength very closely corroborates with the energy band-gap values extracted from the SE measurement (Fig. 8a). Moreover, the Full Width at Half Maximum (FWHM) as measured from the responsivity plot for the as-deposited, 250, 550 and 850 °C annealed samples has been obtained to be 294, 186, 304 and 177 nm, respectively. Therefore, the measured FWHM suggests that the 550 °C annealing will also increase the bandwidth of the photodetector. Furthermore, it is observed that the FWHM of the as-deposited and 550 °C annealed samples are very close to each other. However, it should be noted that the responsivity value of the 550 °C annealed sample has been found to be increased almost ten times as compared to the as-deposited sample. The maximum photoresponse for the 550 °C annealed device is obtained to be ~ 0.09–0.1 A/W which is superior in comparison to the performance of similar heterojunction photodiodes fabricated with CuO-nanowires/Si [40] and by the combination of ZnO and CuO nanowires [5]. The external quantum efficiencies of the fabricated heterojunctions have been plotted in Fig. 12b and it is also observed to be the maximum for the 550 °C annealed sample.

4 Conclusions

CuO thin film has been grown by CBD method and annealed in argon (Ar) environment in a furnace for 10 min at 250, 550 and 850 °C, respectively. Growth kinetics, structure and photo-response of the CuO thin films have been systematically studied with annealing temperature. It has been observed that the annealing temperature has significant impact on the CuO film morphology, amount of CuO phase formed and also on the crystallite quality and size of the

nanostructures. This is attributed to the fact that it gives adequate energy to allow the movement of atoms to occupy the correct site in the crystal lattice. The crystallite size is measured to be the largest (~ 36 nm) for the 550 °C annealed film. The crystalline nature and compositional analysis of the film are determined by XRD and XPS studies and the optical properties are investigated by SE analysis. Annealing the as-deposited CuO film at 550 °C for 10 min in Ar environment has been found to be the best for developing p-CuO/n-Si junction for photo-detection and other optoelectronic applications and has been observed to deliver the best optical and electrical performance compared to the other annealing temperatures considered in the current work. Thus, annealing the CBD grown thin film of p-CuO at 550 °C with average thickness of 110 nm under Ar environment has been found to be a promising low-cost alternative technological route for the development of optoelectronic devices with superior performance.

References

1. G. Awgouropoules, T. Joaminides, C. Papadopoulou, J. Batista, S. Hocever, H.K. Matralis, A comparative study of Pt/γ-Al$_2$O$_3$, Au/α-Fe$_2$O$_3$ and CuO–CeO$_2$ catalyst for the selective oxidation of carbon monoxide in excess hydrogen. Catal. Today **75**, 157–167 (2002)
2. K. Nagase, Y. Zhang, Y. Kodama, J. Kakuta, Dynamic study of the oxidation state of copper in the course of carbon monoxide oxidation over powdered CuO and Cu$_2$O. J. Catal. **187**, 123–130 (1999)
3. J. Sultana, S. Paul, A. Karmakar, R. Yi, G.K. Dalapati, S. Chattopadhyay, Chemical bath deposited (CBD) CuO thin films on n-silicon substrate for electronic and optical applications: impact of growth time. Appl. Surf. Sci. **418**, 380–387 (2016)
4. S. Chandrasekaran, A novel single step synthesis, high efficiency and cost effective photovoltaic applications of oxidized copper nano particles. Sol. Energy Mater. Sol. Cells **109**, 220–226 (2013)
5. S. Wang, C.H. Hsiao, S.J. Chang, Z.Y. Jiao, S.J. Young, S.C. Hung, B.R. Huang, ZnO branched nanowires and the p-CuO/n-ZnO heterojunction nanostructured photodetector. IEEE Trans. Nanotechnol. **12**(2), 263–269 (2013)
6. T. Mahalingam, J.S.P. Chitra, J.P. Chu, H. Moon, H.J. Kwon, Y.D. Kim, Photoelectrochemical solar cell studies on electroplated cuprous oxide thin films. J. Mater. Sci. Mater. Electron. **17**, 519–523 (2006)
7. Z. Jin, X. Zhang, Y. Li, S. Li, G. Lu, 5.1% apparent quantum efficiency for stable hydrogen generation over eosin-sensitized CuO/TiO$_2$ photocatalyst under visible light irradiation. Catal. Commun. **8**, 1267–1273 (2007)
8. L. Fu, J. Gao, T. Zhang, Q. Cao, L.C. Yang, Y.P. Wu, R. Holze, Effect of Cu$_2$O coating on graphite as anode material of lithium

ion battery in PC-based electrolyte. J. Power Sources **171**, 904–907 (2007)

9. Y. Nakamura, H. Zhuang, A. Kishimoto, O. Okada, H. Yanagida, Enhanced CO and CO2 gas sensitivity of the CuO/ZnO heterocontact made by quenched CuO ceramics. J. Electrochem. Soc. **145**, 632–637 (1998)

10. J. Chen, N.Y. Huang, S.Z. Deng, J.C. She, N.S. Xu, W.X. Zhang, X.G. Wen, S.H. Yang, Effects of light illumination on field emission from CuO nanobelt arrays. Appl. Phy. Lett. **86**, 157–159 (2005)

11. P.C. Dai, H.A. Mook, G. Aeppli, S.M. Hayden, F. Dogan, Resonance as a measure of pairing cor-relations in the high-Tc superconductor $YBa_2Cu_3O_{6.6}$. Nature **406**, 965–968 (2000)

12. S. Paul, J. Sultana, A. Karmakar, A. Bhattacharyya, S. Chattopadhyay, Investigation of the comparative photovoltaic performance of n-ZnO nanowire/P-Si and n-ZnO nanowire/p-CuO heterojunctions grown by chemical bath deposition method OPTIK **164**, 745–748 (2018)

13. T. Karlsson, A. Roos, Observation of diffuse interference in reflectance from oxide-coated metals. Sol. Energy Mater. **10**, 105 (1984)

14. D. Wu, Q. Zhang, M. Tao, LSDA+ U study of cupric oxide: electronic structure and native point defects. Phys. Rev. B **73**(23), 206–235 (2006)

15. J.S. Sagu, T.A.N. Peiris, K.G.U. Wijayantha, Rapid and simple potentiostatic deposition of copper (II) oxide thin films. Electrochem. Commun. **42**, 68–71 (2014)

16. J. Sultana, A. Das, A. Das, N.R. Saha, A. Karmakar, S. Chattopadhyay, Characterization of nano-powder grown ultra-thin film p-CuO/n-Si hetero-junctions by employing vapour-liquid-solid method for photovoltaic applications. Thin Solid Films **612**, 331–336 (2016)

17. E.A. Christie, Spectrally selective blacks for energy collection. International Solar Energy Society Conference (1970), pp. 1–7

18. A.O. Musa, T. Akomolafe, M.J. Carter, Production of cuprous oxide, a solar cell material, by thermal oxidation and a study of its physical and electrical properties. Sol. Energy Mater. Sol. Cells **51**, 305–316 (1998)

19. M.A. Brookshier, C.C. Chusuei, D.W. Goodman, Control of CuO particle size on SiO2 by spin coating. Langmuir **15**, 2043–2046 (1999)

20. J.F. Xu, W. Ji, Z.X. Shen, S.H. Tang, X.R. Ye, D.Z. Jia, X.Q. Xin, Preparation of CuO and characterization nanocrystals. J. Solid State Chem. **147**, 516–519 (1999)

21. Y.K. Su, C.M. Shen, H.T. Yang, L. Li, H.J. Gao, Controlled synthesis of highly ordered CuO nano-wire arrays by template based sol–gel route. Trans. Nonferr. Metals Soc. China **17**, 783–786 (2007)

22. X.L. Tang, L. Ren, L.N. Sun, W.G. Tian, M.H. Cao, C.W. Hu, A solvothermal route to Cu_2O nano-cubes and Cu nanoparticles. Chem. Res. Chin. Univ. **22**, 547–551 (2006)

23. C.O. Yuan, H.F. Jiang, C. Lin, S.J. Liao, Shape and size-controlled electrochemical synthesis of cupric oxide nanocrystals. J. Cryst. Growth **303**, 400–406 (2007)

24. J.T. Chen, F. Zhang, J. Wang, G.A. Zhang, B.B. Mian, X.Y. Fan, D. Yan, P.X. Yan, CuO nanowires synthesized by thermal oxidation route. J. Alloy. Compd. **454**, 268–273 (2008)

25. P.K. Nair, M.T.S. Nair, V.M. Garcia, O.L. Arenas, Y. Pena, A. Castillo, I.T. Ayala, O. Gomezdaza, A. Sanchez, J. Campos, H. Hu, R. Suarez, M.E. Rincon, Semiconductor thin films by chemical bath deposition for solar energy related applications. Sol. Energy Mater. Sol. Cells **52**, 313–344 (1998)

26. P.K. Nair, P. Parmananda, M.T.S. Nair, Mathematical model simulating the growth of compound semiconductor thin films via chemical bath deposition. J. Cryst. Growth **206**, 68–74 (1999)

27. L.F. Koao, B.F. Dejene, H.C. Swart, T.E. Motaung, Dependent of reaction time on Cu-doped ZnO nanostructures prepared by chemical bath method. Int. J. Lumin. Appl. **5**, 54–61 (2015)

28. J.Q. Qi, H.Y. Tian, L.T. Li, H.L.W. Chan, Fabrication of CuO nanoparticle interlinked microsphere cages by solution method. Nanoscale Res. Lett. **2**, 107–111 (2007)

29. Z. jian, W. Hejing, The physical meaning of 5 basic parameters for an X-ray diffraction peak and their application. Chin. J. Geochem. **22**, 38–44 (2003)

30. S.L. Mammah, F.E. Opara, V.B.O. Pepple, J.E.E. Ntibi, S.C. Ezugwu, F.I. Ezema, Annealing effect on the optical and solid state properties of cupric oxide thin films deposited using the Aqueous Chemical Growth (ACG) method. Nat. Sci. **5**, 389–399 (2013)

31. K.H. Yoon, W.J. Choi, D.H. Kang, Photoelectrochemical properties of copper oxide thin films coated on an *n*-Si substrate. Thin Solid Films **372**, 250–256 (2000)

32. J.P. Tobin, W. Hirschwald, J. Cunningham, XPS and XAES studies of transient enhancement of Cu^1 at CuO surfaces during vacuum outgassing. Appl. Surf. Sci. **16**, 441–452 (1983)

33. Z. Zhang, P. Wang, Highly stable copper oxide composite as an effective photocathode for water splitting via a facile electrochemical synthesis strategy. J. Mater. Chem. **22**, 2456–2464 (2012)

34. Y.L. Liu, L. Liao, J.C. Li, C.X. Pan, From copper nanocrystalline to CuO nanoneedle array: synthesis, growth mechanism, and properties. J. Phys. Chem. **111**, 5050–5056 (2007)

35. T. Ito, H. Yamaguchi, K. Okabe, T. Masumi, Single-crystal growth and characterization of Cu_2O and CuO. J. Mater. Sci. **33**, 3555–3566 (1998)

36. J. Tang, L. Brzozowski, D.A.R. Barkhouse, X.H. Wang, R. Debnath, R. Wolowiec, E. Palmiano, L. Levina, A.G.P. Abraham, D. Jamakosmanovic, E.H. Sargent, Quantum dot photovoltaics in the extreme quantum confinement regime: the surface-chemical origins of exceptional air-and light-stablity. ACS Nano **4**, 869–878 (2010)

37. R. Sahay, J. Sundaramurthy, P. Suresh Kumar, V. Thavasi, S.G. Mhaisalkar, and S.Ramakrishna, "Synthesis and characterization of CuO nanofibers and investigation for its suitability as blocking layer in ZnO NPs based dye sensitized solar cell and as photocatalyst in organic dye degradation. J. Solid State Chem. **186**, 261–267 (2012)

38. P. Chand, A. Gaur, A. Kumar, U.K. Gaur, Effect of NaOH molar concentration on morphology, optical and ferroelectric properties of hydrothermally grown CuO nanoplates. Mater. Sci. Semicond. Process **38**, 72–80 (2015)

39. Z. Liang, Y. Wang, M. Su, W. Mai, J. Xu, W. Xie, P. Liu, Improving the quality of the Si/Cu_2O interface by methyl-group passivation and its application in photovoltaic devices, Adv. Mater. Interfaces (2017) https://doi.org/10.1002/admi.201600833

40. G. Akgul, F.A. Akgul, E. Mulazimoglu, H.E. Unalan, R. Turan, Fabrication and characterization of copper oxide-silicon nanowire heterojunction photodiodes. J. Phys. D **47**, 1–7 (2014)